Room-Temperature First-Order Phase Transition in a Charge-Disproportionated Molecular Conductor $(MeEDO\text{-}TTF)_2PF_6$

Xiangfeng Shao,*[,†,‡] Yoshiaki Nakano,[†] Masafumi Sakata,[§] Hideki Yamochi,*[,†] Yukihiro Yoshida,[§] Mitsuhiko Maesato,[§] Mikio Uruichi,[||] Kyuya Yakushi,[||] Tsuyoshi Murata,[§] Akihiro Otsuka,[†] Gunzi Saito,[†,§] Shin-ya Koshihara,[‡,⊥] and Koichiro Tanaka[#]

Research Center for Low Temperature and Materials Sciences, Kyoto University, Sakyo-ku, Kyoto 606-8501, Japan, Non-equilibrium Dynamics Project, ERATO, Japan Science and Technology Agency, c/o KEK, 1-1 Oho, Tsukuba, Ibaraki 305-0801, Japan, Division of Chemistry, Graduate School of Science, Kyoto University, Sakyo-ku, Kyoto 606-8502, Japan, Institute for Molecular Science, Okazaki, Aichi 444-8585, Japan, Frontier Collaborative Research Center & Department of Materials Science, Tokyo Institute of Technology, 2-12-1 Oh-okayama, Meguro-ku, Tokyo 152-8551, Japan, and Department of Physics, Graduate School of Science, Kyoto University, Kyoto 606-8224, Japan

Received September 16, 2008

Electrochemical oxidation of 4,5-ethylenedioxy-4′-methyl-tetrathiafulvalene (MeEDO-TTF) afforded three types of $(MeEDO\text{-}TTF)_2PF_6$ radical cation salts under different conditions: black powder, dark green plates, and black plates. The optical absorption spectra of these modifications were very similar to each other. The black powder and dark-green plate modifications were semiconducting and metallic, respectively, and the latter showed a semiconducting behavior below 200 K. The black plate modification exhibited a semiconductor-to-semiconductor first-order phase transition at around room temperature (303 K). The donor molecules in both the high- and low-temperature phases of this modification showed similar packing patterns, based on which the tight-binding approximation afforded similar two-dimensional Fermi surfaces. The phase transition of this modification is accompanied by a subtle change in the relative orientation of the neighboring donor molecules. The vibrational spectra proved that a nearly localized charge disproportionation takes place in the high-temperature phase and the distinct charge disproportionation is developed in the low-temperature phase. These results indicate that the slight lattice distortion assists the stabilization of charge disproportionation. The comparison of the isostructural salts of metallic $(MeEDO\text{-}TTF)_2X$ ($X = BF_4$, ClO_4) and the semiconducting high-temperature phase of the $(MeEDO\text{-}TTF)_2PF_6$ demonstrated that the side-by-side intermolecular interaction is most effectively modulated according to the anion size. The unit cell parameter corresponding to this intermolecular interaction was varied only ca. 2% among these isostructural salts. This observation demonstrates the very sensitive nature of the transport property to the lattice modulation.

Introduction

Since the synthesis of its radical cation in 1970,[1] tetrathiafulvalene (TTF) has remained the most studied heterocyclic system both in the synthetic chemistry and materials sciences in the field of molecular conductors.[2] It is now widely seen that the charge-transfer (CT) complexes of TTF and its derivatives (see Scheme 1) are the gateway to provide molecular semiconductors, metals, and superconductors.[3] Creative efforts have been made and are still ongoing to explore multifunctional molecular conductors based on TTF skeleton.[4] It is widely accepted that the nature of the conducting component plays the most important role in the crystal and electronic structures of the CT complexes.[5] Among the ethylenedioxy-substituted TTF derivatives, bis(ethylenedioxy)-TTF (BO) mainly afforded two-dimensional (2D) stable metallic CT complexes due to its self-assembling nature in the

* Corresponding authors. E-mail: yamochi@kuchem.kyoto-u.ac.jp (H.Y.), shao_xf@hotmail.com (X.S.).
† Research Center for Low Temperature and Materials Sciences, Kyoto University.
‡ Japan Science and Technology Agency.
§ Division of Chemistry, Kyoto University.
|| Institute for Molecular Science.
⊥ Tokyo Institute of Technology.
Department of Physics, Kyoto University.

(1) Wudl, F.; Smith, G. M.; Hufnagel, E. J. *Chem. Commun.* **1970**, 1453–1454.
(2) Yamada, J., Sugimoto, T., Eds. *TTF Chemistry Fundamental and Application of Tetrathiafulvalene*; Kodansha Springer: Tokyo, 2004.
(3) (a) Williams, J. M.; Ferraro, J.; Thorn, R. J.; Carlson, K. D.; Geiser, U.; Wang, H.-H.; Kini, A. M.; Wangbo, M. H. *Organic Superconductors (including Fullerenes)*; Prentice Hall: Englewood Cliffs, NJ, 1992. (b) Ishiguro, T.; Yamaji, K.; Saito, G. *Organic Superconductors*, 2nd ed.; Springer-Verlag: Berlin, 1998.
(4) For comprehensive review, see: (a) *Chem Rev.* **2004**, *104*, Issue 11. (b) *J. Phys. Soc. Jpn.* **2006**, *75*, Issue 5.
(5) Saito, G.; Yoshida, Y. *Bull. Chem. Soc. Jpn.* **2007**, *80*, 1–137.
(6) (a) Horiuchi, S.; Yamochi, H.; Saito, G.; Sakaguchi, K.; Kusunoki, M. *J. Am. Chem. Soc.* **1996**, *118*, 8604–8622. (b) Yamochi, H. Chapter 4 of ref 2.
(7) (a) Ota, A.; Yamochi, H.; Saito, G. *J. Mater. Chem.* **2002**, *12*, 2600–2602. (b) Ota, A.; Yamochi, H.; Saito, G. *J. Low. Temp. Phys.* **2006**, *142*, 425–428. (c) Ota, A.; Yamochi, H.; Saito, G. In *Multifunctional Conducting Molecular Materials*; Saito, G., Wudl, F., Haddon, R. C., Tanigaki, K., Enoki, T., Katz, H. E., Maesato, M., Eds.; RSC Publishing: Cambridge, U.K., 2007; pp 115−118.

10.1021/cm802517s CCC: $40.75
Published on Web 11/18/2008

Scheme 1. Chemical Structures of the Molecules Described in This Paper[a]

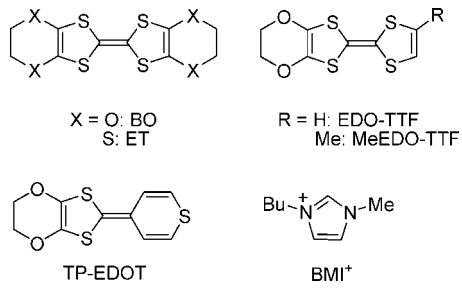

[a] ET: bis(ethylenedithio)-TTF.

partially oxidized states.[6] Ethylenedioxy-TTF (EDO-TTF), a donor molecule derived from BO by removal of one of the ethylenedioxy groups, afforded complexes with a variety of electronic ground states, and the BO-type self-assembling ability was greatly diminished.[7]

It is of increasing interests in the material sciences to investigate the sensitivities of their electronic states to the external stimuli. Regarding molecular CT complexes, the melting of the charge ordering (CO) state by the electric field[8] and light,[9] as well as the suppression or collapse of the CO state by pressure into metallic or superconducting state,[10] is the latest fascinating issue in both fundamental and applied sciences. Recently, we reported the melting of the CO state by a laser pulse in a 1/4-filled quasi-one-dimensional organic conductor $(EDO\text{-}TTF)_2PF_6$.[11] This material shows an ultra-fast and highly efficient photo-induced phase transition (PIPT) in which one photon converts ca. 500 donor molecules within a response time of 1.5 ps. This material has potential for use in an ultrafast switching system. Strong electron−phonon (molecular vibration) coupling was regarded as one of the origins of this peculiar phenomenon. In other words, the relatively small-sized and flexible π-electron system in EDO-TTF play important roles in the PIPT of $(EDO\text{-}TTF)_2PF_6$. Although the conformational modulation of the conjugated system is mainly noted in this example, the displacements of conducting component molecules in a crystal must be considered to investigate the functionalities of molecular materials. In connection with the latter viewpoint among relatively small sized π-electron systems having ethylenedioxy group, the sensitivity of the physical properties to the modulations of the crystal structure of $(TP\text{-}EDOT)_3Sb_2F_{11}$(Benzene) (TP-EDOT: 2-(thiapyran-4-ylidene)-4,5-ethylenedioxy-1,3-dithiole) is worth noting. This material showed a diamagnetic semiconducting behavior, while the crystal structure analysis suggested a paramagnetic one. The origin of the discrepancy was interpreted on the basis of the sensitivity of the electronic structure on the crystal structure modulation.[12]

These results indicate that donor molecules with small π-electron systems and the ethylenedioxy-1,3-dithiole group have the potential to provide CT complexes showing a sensitive feature to external stimuli and/or structural modulation. To explore the switching system further, a minor chemical modification of EDO-TTF was carried out by introducing one methyl group to afford 4-methyl-EDO-TTF (MeEDO-TTF), of which the electronic structure of the π-conjugated system was similar to that of EDO-TTF.[13] Our previous investigation revealed that the introduction of a methyl group into EDO-TTF suppressed face-to-face type intermolecular interactions. Among the complexes, $(MeEDO\text{-}TTF)_2X$ ($X = BF_4$, ClO_4) showed metallic behavior due to its two-dimensional electronic structure despite the weak intermolecular interactions between the donor molecules.[13] These salts, however, are considered to be located close to the border between metal and semiconductor since the magnitudes of the intermolecular interactions are relatively small. Therefore, the modulations of the intermolecular overlap integrals and other parameters by means of the chemical modification of the counter components are expected to provide the conductors with phase transition, that is, the switching materials.

(8) (a) Potember, R. S.; Poehler, P. O.; Cowan, D. O. *Appl. Phys. Lett.* **1979**, *34*, 405–407. (b) Tokura, Y.; Okamoto, H.; Koda, T.; Mitani, T.; Saito, G. *Phys. Rev. B* **1988**, *38*, 2215–2218. (c) Tomić, S.; Cooper, J. R.; Jérome, D.; Bechgaard, K. *Phys. Rev. Lett.* **1989**, *62*, 462–465. (d) Iwasa, Y.; Koda, T.; Koshihara, S.; Tokura, Y.; Iwasawa, N.; Saito, G. *Appl. Phys. Lett.* **1989**, *55*, 2111–2113. (e) Iwasa, Y.; Koda, T.; Koshihara, S.; Tokura, Y.; Iwasawa, N.; Saito, G. *Phys. Rev. B* **1989**, *39*, 10441–10444. (f) Watanabe, N.; Iwasa, Y.; Koda, T. *Phys. Rev. B* **1991**, *44*, 11111–11118. (g) Kumai, R.; Okimoto, Y.; Tokura, Y. *Science* **1999**, *284*, 1645–1647. (h) Toyota, N.; Abe, Y.; Kuwabara, T.; Negishi, E.; Matsui, H. *J. Phys. Soc. Jpn.* **2003**, *72*, 2714–2717. (i) Sawano, F.; Terasaki, I.; Mori, H.; Mori, T.; Watanabe, M.; Ikeda, N.; Nogami, Y.; Noda, Y. *Nature* **2005**, *437*, 522–524. (j) Matsushita, M. M.; Sugawara, T. *J. Am. Chem. Soc.* **2005**, *127*, 12450–12451. (k) Okamoto, K.; Tanaka, T.; Fujita, W.; Agawa, K.; Inabe, T. *Angew. Chem., Int. Ed. Engl.* **2006**, *45*, 4516–4518.

(9) (a) Koshihara, S.; Tokura, Y.; Iwasa, Y.; Koda, T.; Saito, G.; Mitani, T. *Synth. Met.* **1991**, *42*, 2351–2354. (b) Collet, E.; Lemée-Caileau, M.-H.; Buron-Le Cointe, M.; Caileau, H.; Wulff, M.; Luty, T.; Koshihara, S.; Meyer, M.; Toupet, L.; Rabiller, P.; Techert, S. *Science* **2003**, *300*, 612–615. (c) Naito, T.; Inabe, T.; Niimi, H.; Asakura, K. *Adv. Mater.* **2004**, *16*, 1786–1790. (d) Tajima, N.; Fujishima, J.; Naka, N.; Ishihara, T.; Kato, R.; Hishio, Y.; Kajita, K. *J. Phys. Soc. Jpn.* **2005**, *74*, 511–514. (e) Koshihara, S.; Adachi, S. *J. Phys. Soc. Jpn.* **2006**, *75* (1), 011005.

(10) (a) Bourbonnais, C.; Jérome, D. *Science* **1998**, *281*, 1155–1156. (b) Vescoli, V.; Degiorgi, L.; Henderson, W.; Grüner, G.; Starkey, K. P.; Montgomery, K. L. *Science* **1998**, *281*, 1181–1184. (c) Kishine, J.; Yonemitsu, K. *Int. J. Mod. Phys. B* **2002**, *16*, 711–771. (d) Biermann, S.; Georges, A.; Giamarchi, T.; Lichtenstein, A. *Proceedings of the NATO ASI "Field Theory of Strongly Correlated Fermions and Bosons in Low-Dimensional Disordered Systems"*, Windsor, August 2001, arXiv:cond-mat/0201542v1. (e) Itou, T.; Kanoda, K.; Murata, K.; Matsumoto, T.; Hiraki, K.; Takahashi, T. *Phys. Rev. Lett.* **2004**, *93*, 216408/1-4. For some examples of the pressure-induced charge-ordering state to superconducting state, see (f) Kimura, S.; Maejima, T.; Suzuki, H.; Chiba, R.; Mori, H.; Kawamoto, T.; Mori, T.; Moriyama, H.; Nishio, Y.; Kajita, K. *Chem. Commun.* **2004**, 2454–2455. (g) Kobayashi, A.; Suzumura, Y.; Higa, M.; Kondo, R.; Kagoshima, S.; Nishikawa, H. *J. Phys.: Condens. Matter* **2008**, *20*, 125205. (h) Nishikawa, H.; Morimoto, T.; Kodama, T.; Ikemoto, I.; Kikuchi, K.; Yamada, J.; Yoshino, H.; Murata, K. *J. Am. Chem. Soc.* **2002**, *124*, 730–731. (i) Nishikawa, H.; Sato, Y.; Kikuchi, K.; Kodama, T.; Ikemoto, I.; Yamada, J.; Oshio, H.; Kondo, R.; Kagoshima, S. *Phys. Rev. B* **2005**, *72*, 052510/1-4. (j) Tajima, N.; Ebina-Tajima, A.; Tamura, M.; Nishio, Y.; Kajita, K. *J. Phys. Soc. Jpn.* **2002**, *71*, 1832–1835.

(11) (a) Uchida, N.; Koshihara, S.; Ishikawa, T.; Ota, A.; Fukuya, H. S.; Collet, M.; Yamochi, H.; Saito, G. *J. Phys. IV France* **2004**, *114*, 143–145. (b) Collet, M.; Guerin, L.; Uchida, N.; Fukuya, S.; Shimoda, H.; Ishikawa, T.; Matsuda, K.; Hasegawa, T.; Ota, A.; Yamochi, H.; Saito, G.; Tazaki, R.; Adachi, S.; Koshihara, S. *Science* **2005**, *307*, 86–89.

(12) Yamochi, H.; Hagiwara, J.; Soeda, M.; Saito, G. *J. Mater. Chem.* **2006**, *16*, 550–557.

(13) Shao, X.; Nakano, Y.; Yamochi, H.; Dubrovskiy, A. D.; Otsuka, A.; Murata, T.; Yoshida, Y.; Saito, G.; Koshihara, S. *J. Mater. Chem.* **2008**, *18*, 2131–2140.

Table 1. Experimental Conditions for the Preparation of Three Modifications of (MeEDO-TTF)$_2$PF$_6$

modification	donor, mg	electrolyte, mg	solvent, mL	current, μA	time, day	yield, mg	appearance
1[a]	MeEDO-TTF, 10.5	$(Bu_4N)PF_6$, 98	EtOH, 17	0.5	7−10	6.1	black powder
2	MeEDO-TTF, 6.3	$(BMI)PF_6$, 120	*n*-propanol, 18	0.5	7−10	4.4	dark-green plate
3	MeEDO-TTF, 6.2	$(BMI)PF_6$, 70	*n*-propanol, 18	0.5	7−10	3.4	black plate
	MeEDO-TTF, 6.6	$(BMI)PF_6$, 90	EtOH, 18	0.5	7−10	3.7	black plate

[a] See ref 13.

Table 2. Optical Absorption Spectra, Transport and Magnetic Properties of (MeEDO-TTF)$_2$PF$_6$

		transport property[a]		
modification	optical spectra (10^3 cm^{-1})	σ (S cm^{-1})	E_a (meV)	magnetic susceptibility (10^{-4} emu spin^{-1})
1	3.1, 14, 32	3 (300 K), S	100 (300 K)	3.9 (300 K)
2	3.2, 14, 33	30 (300 K), T_{MI} = 200 K	16 (140 K)	2.3 (300 K)
3	3.1, 14, 31	4 (305 K), S	34 (305 K)	4.5 (305 K)
		0.07 (300 K), S	400 (300 K)	5.4 (300 K)

[a] S: semiconductor; T_{MI}: metal-to-insulator transition temperature.

This paper reports the structures and physical properties of MeEDO-TTF salts with PF_6 anion, the size of which is slightly larger than those of BF_4 and ClO_4 (Scheme 1). Although this study was initiated to improve the crystal quality of the previously reported semiconducting 2:1 salt,[13] three polymorphs were obtained. In this report, special emphasis is given to the black plate modification, as it shows a semiconductor-to-semiconductor phase transition due to the modulation of the charge localization. The salt also demonstrated the border between metallic and semiconducting state of a series of charge-disproportionated radical cation salts.

Results and Discussion

Preparation of Radical Cation Salts. Recently, we reported that the electrochemical oxidation of MeEDO-TTF in the presence of $(Bu_4N)PF_6$ in EtOH afforded a black powdery radical cation salt (**1**), which was a semiconductor with good conductivity at room temperature (σ_{rt} = 3 S cm^{-1}).[13] Attempts to obtain the single crystals of the radical cation salt by employing $(Bu_4N)PF_6$ under various experimental conditions ended in failure; the application of low-polarity solvents, controlling the temperature, changing the shape and volume of the electrochemical cells, adjusting the applied current, and other methods did not yield single crystals. When an ionic liquid $(BMI)PF_6$ (BMI: 1-butyl-3-methylimidazolium)[14] was employed as electrolyte, however, crystalline products were obtained. In this case, the concentration of an electrolyte and choice of solvent affected the product, as summarized in Table 1 (see also Figure S1 in Supporting Information). For example, when *n*-propanol was used as a solvent, two types of radical cation salts, dark-green plates (**2**) and black plates (**3**), were obtained exclusively under high and low concentrations of $(BMI)PF_6$, respectively. When EtOH was applied as a solvent, a similar tendency was observed, while the high concentration of the supporting electrolyte resulted in the production of the mixture of **2** and **3**. Since superior crystal quality was obtained from the electrocrystallization in EtOH, this solvent was employed for the preparation of **3** for structural analysis and physical property measurements. These three modifications had the same donor:anion ratio of 2:1, which was estimated on the basis of the elemental analyses for **1** and **2**, while that of **3** was confirmed by X-ray single crystal structure analysis. As for the other octahedral anions (AsF_6, SbF_6, NbF_6, etc.), so far, no single crystals of good qualities for this kind of investigation were available, though they are important for comparison.

The formation of polymorphs has rarely been observed for the salts of ethylenedioxy-substituted TTF derivatives (EDO-TTF and BO), while bis(ethylenedithio)-TTF (ET) is known to provide polymorphic products; e.g., $(ET)_2I_3$ has been reported to form at least four different phases.[15] In addition, it is noteworthy that the polymorphism was observed in the radical cation salts of MeEDO-TTF with the ReO_4 anion.[16] These results demonstrate that the nature of MeEDO-TTF resembles that of ET regarding the polymorphism of the cation radical salts despite the fact that the former is an EDO-TTF derivative.

Optical Absorption Spectra. The optical absorption spectra were measured by dispersing the radical cation salts in KBr pellets. These three modifications showed similar optical spectra especially below 25 × 10^3 cm^{-1} as summarized in Table 2 (see also Figure S2 in Supporting Information). As a typical example, the spectrum of **3** is shown in Figure 1. The lowest energy absorption band (A band) appeared at around 3.1 × 10^3 cm^{-1}, which is almost the same position as that observed in the previously reported metallic $(MeEDO\text{-}TTF)_2X$ (X = BF_4, ClO_4) salts.[13] This A

(14) Ionic liquid was successfully used in the preparation of the organic radical cation salts of TTF and its derivatives. For example, the preparations of superconductor $(TMTSF)_2NbF_6$ and Mott insulator α′-$(ET)_2(H_2F_3)$ were reported in refs a and b, respectively. (a) Sakata, M.; Yoshida, Y.; Maesato, M.; Saito, G.; Matsumoto, K.; Hagiwara, R. *Mol. Cryst. Liq. Cryst.* **2006**, *452*, 103–112. (b) Yoshida, Y.; Sakata, M.; Saito, G.; Matsumoto, K.; Hagiwara, R. *Chem. Lett.* **2007**, *36*, 226–227.

(15) (a) Williams, J. M.; Schultz, A. J.; Geiser, U.; Carlson, K. D.; Kini, A. M.; Wang, H. H.; Kwok, W.-K.; Wangbo, M.-H.; Schirber, J. E. R. *Science* **1991**, *252*, 1501–1508. (b) Carlson, K. D.; Wang, H. H.; Beno, M. A.; Kini, A. M.; Williams, J. M. *Mol. Cryst. Liq. Cryst.* **1990**, *181*, 91–104.

(16) Shao, X.; Yoshida, Y.; Nakano, Y.; Yamochi, H.; Khasanov, S.; Sakata, M.; Maesato, M.; Otsuka, A.; Saito, G.; Koshihara, S. To be submitted to *Chem. Mater.*

(17) For reviews, see. (a) Jacobsen, C. S. In *Semiconductors and Semimetals: Highly Conducting Quasi-One-Dimensional Organic Crystals*; Conwell, E., Ed.; Academic Press, Inc.: New York, 1988; Vol *27*, Chapter 5, pp 306, 317. (b) Torrance, J. B. *Acc. Chem. Res.* **1979**, *12*, 79–86.

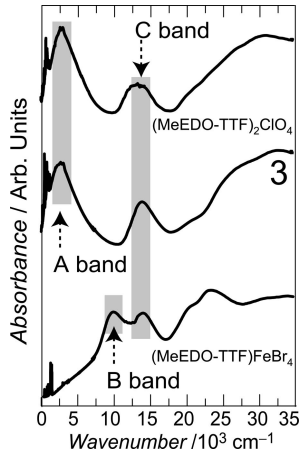

Figure 1. Optical absorption spectrum of **3** at room temperature, along with the spectra of the metallic salt (MeEDO-TTF)$_2$ClO$_4$ and monocationic salt (MeEDO-TTF)FeBr$_4$ in KBr pellets. See text for details of the A, B, and C bands.

band is assigned to the intermolecular CT transition: $D^0 + D^{\bullet+} \rightarrow D^{\bullet+} + D^0$, where D indicates the donor. The existence of this band is, in general, indicative of the metallic or highly conducting behavior at room temperature.[17] Another type of intermolecular CT absorption band assigned to the transition of $D^{\bullet+} + D^{\bullet+} \rightarrow D^{2+} + D^0$ (B band), which appeared at around 10×10^3 cm^{-1} for the monocationic (MeEDO-TTF)FeBr$_4$ salt, was not observed in all modifications of PF_6 salts in this study. The C band and the other high-energy absorption bands observed for all of these salts were assigned to the intramolecular transitions of MeEDO-TTF.[13]

Transport and Magnetic Properties. Since **2** was obtained as very thin and extremely fragile plates, the temperature-dependent resistivity (ρ) measurements for this salt and **1** were carried out on compressed pellets, while that of **3** was performed on a single crystal. The transport and magnetic properties of these three modifications are summarized in Table 2.

2 showed good conductivity of 30 S cm^{-1} at room temperature and a weak metallic behavior down to 200 K associated with a Pauli-like paramagnetism (Figure 2a). Below 200 K, this salt exhibited a semiconducting behavior with small activation energy, for example, 16 meV at 140 K. Since the Pauli-like paramagnetic behavior was maintained down to 50 K, the intrinsic transition temperature of this salt should be lower than that determined by conductivity measurements. The physical properties of **2** are similar to those of the other MeEDO-TTF salts which show metal-to-insulator (MI) transitions, such as (MeEDO-TTF)$_2$X (X = AsF_6, SbF_6).[13]

Although **3** exhibited semiconducting behavior in the entire measured temperature range (340−110 K), an abrupt change of the resistivity was observed at around 304 K for heating and 302 K for cooling, indicating a semiconductor-to-semiconductor first-order phase transition (Figure 2b,c). The activation energies for the electric conduction of the higher-temperature high-conducting phase (*H*-phase) and lower-temperature low-conducting phase (*L*-phase) were 34 and 400 meV, respectively. The conductivity enhancement between the *H*- and *L*-phases was around 60 times. The

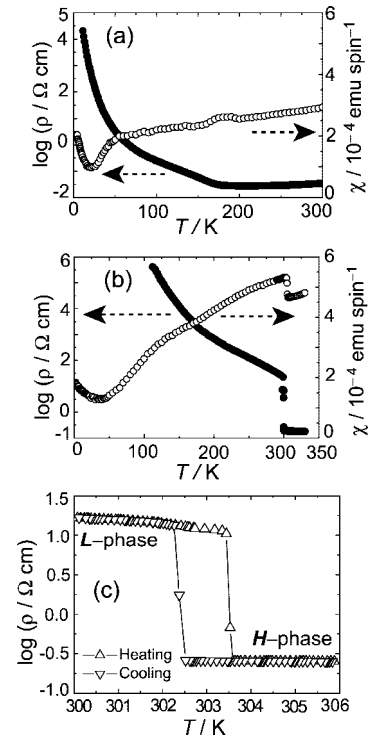

Figure 2. Temperature-dependent resistivity ρ (closed circle) and static magnetic susceptibility χ (open circle) of **2** (a) and **3** (b). The left and right axes in each panel indicate the log(ρ) and χ, respectively. (c) Hysteresis loop of the temperature-dependent resistivity of **3**.

temperature dependences of the magnetic susceptibility (χ) of **3** on the heating and cooling processes also showed jumps at around 304 K. The tendency of the $\chi-T$ plot at high-temperature region (T > 305 K) was similar to those of stable metallic (MeEDO-TTF)$_2$X (X = BF_4, ClO_4) salts, although the data were collected only in the narrow temperature range from 305 to 330 K. The χ of the *L*-phase (T < 304 K) showed larger value than that of the *H*-phase at the transition temperature (see Table 2) and exhibited a monotonic decrement on cooling. The relatively high χ value at around room temperature suggests a localized feature due to the strong electron correlation in this salt. The existence of the interconvertible bistable states (*H*- and *L*-phases) indicates that **3** has the potential to be used in the molecular switching and/or memory system near the room temperature.

Crystal and Electronic Structures. Among the three polymorphs, only the black plate modification, **3**, gave the single crystals adequate for structural analysis. The temperature variation of the crystallographic data is summarized in Table 3. On heating, the structure of the *L*-phase was observed in the temperature range of 110−302 K, while on cooling, the structure corresponded to the *H*-phase in the temperature range of 342−302 K. Hence, the structures for both the *H*- and *L*-phases could be compared at the same temperature of 302 K.

Figure 3a depicts the *c*-axis projection of the crystal structure of the *H*-phase. In both the *H*- and the *L*-phases, the asymmetric unit contained one donor and one-half of the anion. Salt **3** showed a layered structure in both phases: the conducting layers consisting of MeEDO-TTF molecules were sandwiched by the layers of the octahedral anion PF_6. The main difference in the conducting layers between the

Table 3. Crystal Data, Data Collection, and Refinement Parameters for Structure Analysis of 3

	L-phase			*H*-phase	
	110 K	290 K	302 K (heating)	302 K (cooling)	320 K
chemical formula	$C_{18}H_{16}O_4S_8PF_6$	$C_{18}H_{16}O_4S_8PF_6$	$C_{18}H_{16}O_4S_8PF_6$	$C_{18}H_{16}O_4S_8PF_6$	$C_{18}H_{16}O_4S_8PF_6$
formula weight	697.76	697.76	697.76	697.76	697.76
crystal system	orthorhombic	orthorhombic	orthorhombic	orthorhombic	orthorhombic
space group	*Pbcn*	*Pbcn*	*Pbcn*	*Cmcm*	*Cmcm*
crystal size, mm^3	0.7 × 0.25 × 0.05	0.7 × 0.25 × 0.05	0.7 × 0.25 × 0.05	0.7 × 0.25 × 0.05	0.7 × 0.25 × 0.05
absorption coefficient, mm^{-1}	0.853	0.819	0.816	0.799	0.795
a, Å	29.142(2)	29.467(4)	29.487(4)	29.676(4)	29.695(4)
b, Å	12.557(1)	12.642(2)	12.665(2)	12.596(2)	12.614(2)
c, Å	6.8170(2)	6.9760(5)	6.9850(5)	6.9920(5)	7.0070(5)
V, Å^3	2495.2(3)	2598.7(6)	2608.4(6)	2613.6(5)	2624.6(5)
Z	4	4	4	4	4
d_{calcd}, g cm^{-3}	1.857	1.784	1.777	1.677	1.670
radiation	Mo Kα	Mo Kα	Mo Kα	Mo Kα	Mo Kα
$2\theta_{max}$, °	52.4	52.3	52.3	52.0	52.1
independent observed reflections	2210	2156	2142	1403	1405
reflections with $I > 2\sigma(I)$	1915	1496	1438	1078	1051
no. of refined parameters	200	227	227	143	143
R^a	0.037	0.043	0.043	0.065	0.061
$wR2^b$	0.1052	0.1221	0.1188	0.2025	0.2008
goodness of fit^c	1.152	1.028	1.051	1.064	1.043

[a] Calculated only for the reflections with $I > 2\sigma(I)$ [b] Calculated for all of the independent reflections, $W = 1/[\sigma^2F^2 + (\alpha P)^2 + \beta P]$, where $P = (F_0^2 + 2F_c^2)/3$; at 110 K, $\alpha = 0.0575$, $\beta = 1.8481$; at 290 K, $\alpha = 0.0548$, $\beta = 2.0434$; at 302 K (heating), $\alpha = 0.0538$, $\beta = 1.1639$; at 302 K (cooling), $\alpha = 0.1156$, $\beta = 9.3363$; at 320 K, $\alpha = 0.1261$, $\beta = 3.6223$. [c] Calculated for all of the independent reflections.

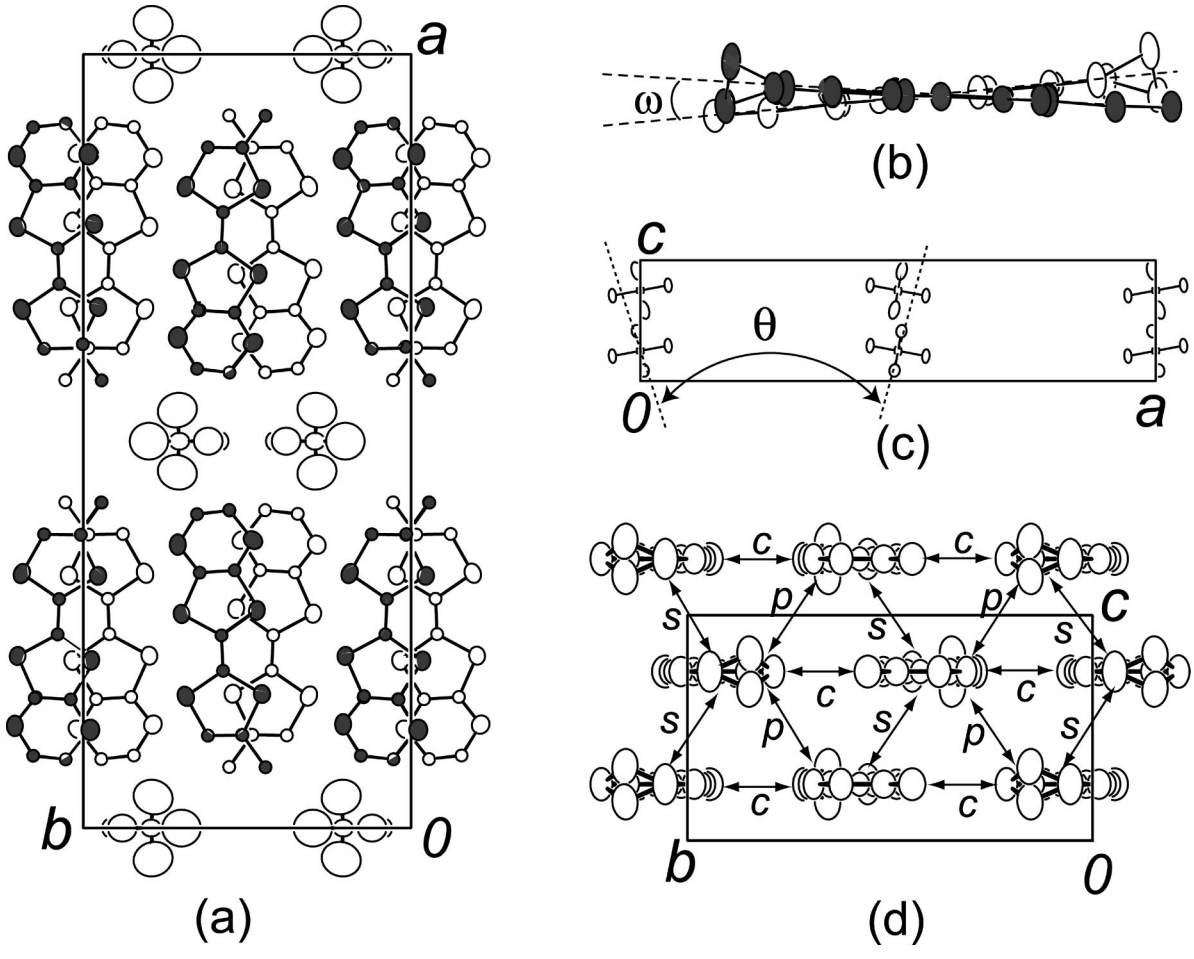

Figure 3. Crystal structure of **3**. The hydrogen atoms are omitted for clarity. (a) Crystal structure projected onto the *ab*-plane with the donor molecules at $z = 1/4$ shown in gray. Although this figure depicts the molecular packing in the *H*-phase (302 K), that of the *L*-phase is almost identical to this illustration except for the thermal ellipsoids of fluorine atoms. (b) Projection along the molecular short axis of two neighboring donor molecules in the *L*-phase, where ω indicates the twisting angle. The atoms of the top molecule are shaded. (c) Anion arrangement on the *ac*-plane in the *L*-phase (110 K). The dashed line indicates the best plane of the equator of the uniaxial rotation, where θ is the dihedral angle between the equator planes for the anions at $x = 0$ and $x = 1/2$. (d) View of the donor layer at $x = 1/4$ along the *a*-axis with the scheme of the intermolecular overlap integrals for the *H*- and *L*-phases at 302 K. For the numerical values of the intermolecular the overlap integrals, see Table 4.

Table 4. Comparison of the Anion Size (V_A), Lattice Constants (a, b, c), Intermolecular Overlap Integrals (c, s, p), and Bandwidths (W) for (MeEDO-TTF)$_2$X (X = BF$_4$, ClO$_4$, PF$_6$)

salt	transport property[a]	V_A, Å^3	a, Å	b, Å	c, Å	c, 10^{-3}	s, 10^{-3}	p, 10^{-3}	W, eV
(MeEDO-TTF)$_2$BF$_4$	*M*	89.5	28.752(2)	12.368(1)	6.969(1)	11.8	−5.1	8.3	0.80
(MeEDO-TTF)$_2$ClO$_4$	*M*	97.5	29.107(3)	12.412(1)	6.962(1)	11.3	−5.2	8.5	0.79
3, *H*-phase (302 K)	*S*	112.8	29.676(4)	12.596(2)	6.9920(5)	−9.9	4.9	8.5	0.74
3, *L*-phase (302 K)	*S*	112.8	29.487(4)	12.665(2)	6.9850(5)	9.2	4.9	−8.5	0.70

[a] *M*: Metallic down to 10 K; *S*: semiconducting.

H- and the *L*-phases appeared in the relative orientation along the molecular short axis. The mean planes of the neighboring donor molecules in the *H*-phase were parallel to each other, while those in the *L*-phase were twisted with an angle of $\omega = 4°$ at 302 K (Figure 3b), which was slightly increased to 6° at 110 K.

In the structural transition of **3**, the disorder mode of the anion was obviously modulated. The anion showed an isotropic rotational disorder in the *H*-phase, while a uniaxial rotation was observed in the *L*-phase. In the latter, although a precessional feature was observed at around room temperature, the direction of the rotational axis was fixed in the lower-temperature region and the uniaxial rotation was suppressed at 110 K (Figure 3c and Figure S3 in Supporting Information). The equators of the rotation for the anions at $x = 0$ and 1/2 showed the dihedral angle of 19.9° at 302 K, which showed no distinct change on cooling (20.8° at 110 K).

The donor packing patterns for both the *H*- and the *L*-phases were rather similar to each other. In the *H*-phase, the donor molecules were located on the mirror planes at $z = 1/4$ (and 3/4) to show the completely planar conformation of the π-conjugated system, while one of the terminal ethylene carbon atoms was out of the plane and disordered. The donor packing pattern was isostructural to those of stable metallic salts (MeEDO-TTF)$_2$X (X = BF$_4$, ClO$_4$) except that both of the ethylene carbon atoms were disordered in the latter case. One donor molecule was surrounded by six neighboring donors in the 0, 60, and 120° directions with respect to the molecular short axis (Figure 3d). Along the 0° direction (parallel to the *b*-axis), stripes of MeEDO-TTF molecules were formed on the mirror plane in which multiple intermolecular atomic contacts shorter than or close to the sums of van der Waals (vdW) radii[18] were observed (Figure 4). The molecular long axes of head-to-head neighboring donor molecules along the *c*-axis (intermolecular overlap integral *s* in Figure 3d) were twisted by around 5°, similarly to those in the isostructural BF$_4$ and ClO$_4$ salts. Comparing the overlap integrals calculated for the 0, 60, and 120° directions, the first one, *c*, showed the largest magnitude but less than 10×10^{-3}. Along the 60 and 120° directions, the intermolecular interactions, *s* and *p*, were smaller than but comparable to that along the 0° direction. The intermolecular interactions were somewhat smaller than those calculated for BF$_4$ and ClO$_4$ salts, especially for *c* (Table 4).

In the *L*-phase, an approximately planar donor molecule was in the general position, and the terminal ethylene group was ordered even at 302 K. The intermolecular interactions along the 60 and 120° directions, *s* and *p*, showed almost

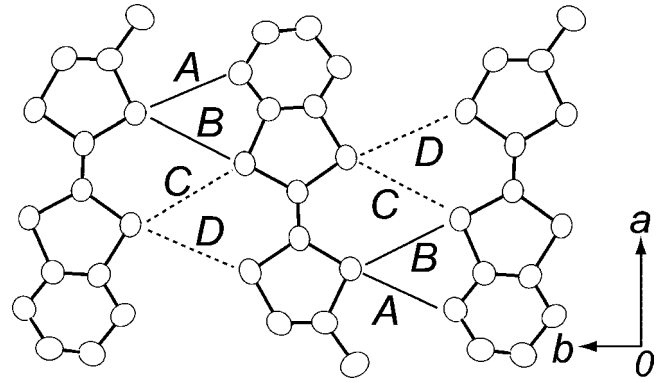

Figure 4. Intermolecular side-by-side contacts of **3** in the *H*-phase at 302 K. Those of the *L*-phase are in the same mode. Solid lines indicate contacts shorter than the sum of the van der Waals radii (vdW: S, 1.80; O, 1.52 Å), while dashed lines show those slightly longer than the sum of the vdW radii. For the *H*-phase, $A = 3.290(6)$, $B = 3.524(7)$, $C = 3.791(8)$, $D = 3.757(6)$ Å; for the *L*-phase, $A = 3.311(4)$, $B = 3.550(4)$, $C = 3.821(5)$, $D = 3.803(5)$ Å.

the same values to those of the *H*-phase, while that along the 0° direction, *c*, was smaller than that of the *H*-phase. Corresponding to the reduction of the side-by-side interaction, the calculated bandwidths were narrowed from 0.74 eV for the *H*-phase to 0.70 eV for the *L*-phase.

Similar to those of stable metallic salts (MeEDO-TTF)$_2$X (X = BF$_4$, ClO$_4$), the tight binding calculations provided 2D electronic structures for both of the *H*- and *L*-phases of **3** as shown in Figure 5. To understand the discrepancy between the calculated metallic electronic structure and the experimentally observed semiconducting behavior, the vibrational spectra were studied. In the next section the spectra of neutral and monocationic MeEDO-TTF are analyzed, and then the temperature-dependent Raman spectra of **3** are discussed.

Origin of the Semiconducting Behavior of 3. *Infrared Spectra.* As is well-known, the frequency shifts of C=C stretching vibrations have been utilized to determine the charge on the component molecules in CT complexes such as TTF,[19] ET,[20] and BO.[21] In this study, the normal-mode analyses of neutral MeEDO-TTF^0 and monocationic MeEDO-TTF$^+$ were carried out at the B3LYP/6-31G(d,p) level of theory to make assignments of the vibrational spectra. Full-geometry optimizations were performed to afford the nonplanar MeEDO-TTF^0 and the planar MeEDO-TTF$^+$. The

(18) Bondi, A. *J. Phys. Chem.* **1964**, *68*, 441–451.

(19) Mstsuzaki, S.; Moriyama, T.; Toyoda, K. *Solid State Commun.* **1980**, *34*, 857–859.

(20) (a) Wang, H. H.; Ferraro, J. R.; Williams, J. M.; Geiser, U.; Schlueter, J. A. *J. Chem. Soc., Chem. Commun.* **1994**, 1893–1894. (b) Yamamoto, T.; Uruichi, M.; Yamamoto, K.; Yakushi, K.; Kawamoto, A.; Taniguchi, H. *J. Phys. Chem. B* **2005**, *109*, 15226–15235.

(21) Drozdova, O.; Yamochi, H.; Yakushi, K.; Uruichi, M.; Horiuchi, S.; Saito, G. *J. Am. Chem. Soc.* **2000**, *122*, 4436–4442.

(22) (a) Demiralp, E.; Dasgupta, S.; Goddard, W. A., III *J. Am. Chem. Soc.* **1995**, *117*, 8154–8158. (b) Demiralp, E.; Dasgupta, S.; Goddard, W. A., III *J. Phys. Chem. A* **1997**, *101*, 1975–1981.

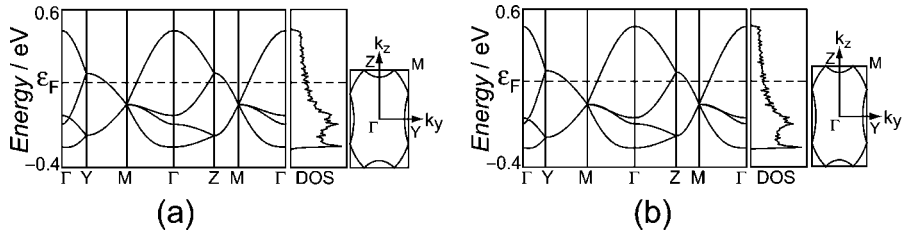

Figure 5. Calculated band dispersion, density of states (DOS), and Fermi surface of **3** for (a) the *H*- and (b) *L*-phases.

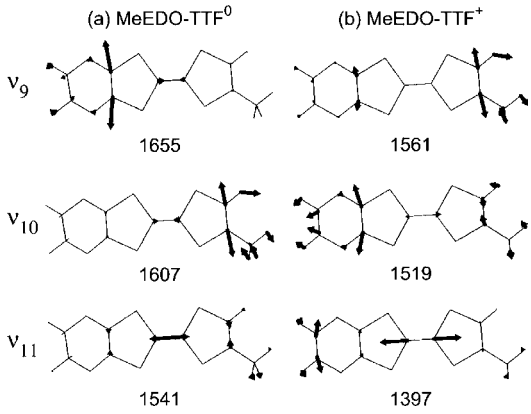

Figure 6. C═C stretching modes of (a) MeEDO-TTF^0 and (b) MeEDO-TTF$^+$ calculated at the B3LYP/6-31G(d,p) level. Calculated frequencies (cm^{-1}) are also shown. As for the other modes, see Table S1 in Supporting Information.

tendency of the charge-dependent molecular shape is similar to those of TTF derivatives such as ET,[22] BO,[23] BDH-TTP,[24] and EDO-TTF.[25] The calculated 63 modes including frequencies, infrared intensities, and Raman activities are listed in Table S1 in Supporting Information. The normal-mode analysis reproduced the experimental spectra at the acceptable level by applying the scaling factor of 0.96 to calculated frequencies (See Supporting Information, Table S2).

Three C═C stretching modes of MeEDO-TTF^0 and MeEDO-TTF$^+$ are shown in Figure 6. The ν_9 and ν_{10} modes are approximately regarded as in-phase and out-of-phase stretching modes of wing C═C bonds, respectively. The ν_{11} mode is mainly dominated by the central C═C stretching mode. In contrast to symmetrical BEDT-TTF and BEDO-TTF, all of these C═C stretching vibrations can be observed in both infrared and Raman spectra due to the low symmetry of the MeEDO-TTF molecule.

The infrared spectra of MeEDO-TTF and (MeEDO-TTF)FeBr$_4$ in the C═C stretching region are shown in Figure 7 and Table 5. In this spectral region, CH_2 scissoring (ν_{12} and ν_{14}), CH_3 bending (ν_{13}, ν_{15}, and ν_{16}), CH_2 wagging (ν_{17} and ν_{18}), and CH_2 twisting (ν_{19} and ν_{20}) modes were observed in the neighborhood of C═C stretching (ν_9, ν_{10}, and ν_{11}) modes. However, the pair of ν_9 and ν_{10} modes was easily distinguished from other bands based on the frequencies and intensities. By oxidizing MeEDO-TTF from neutral to +1, the relative intensities of ν_9 and ν_{10} modes were reversed

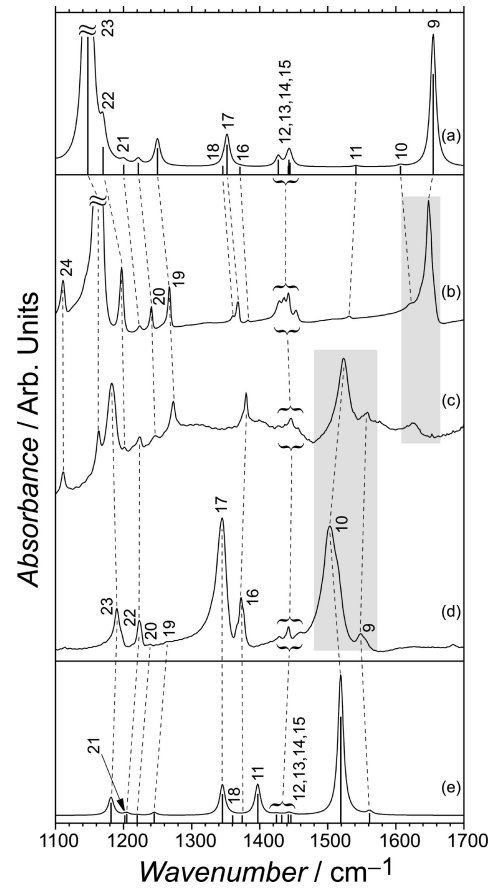

Figure 7. (a) Calculated and (b) observed infrared spectra of MeEDO-TTF. (c) Observed infrared spectrum of (MeEDO-TTF)$_2$PF$_6$ (**3**). (d) Observed and (e) calculated infrared spectra of (MeEDO-TTF)FeBr$_4$. Calculations were carried out at the B3LYP/6-31G(d,p) level of theory. Numbering of the bands corresponds to that of fundamental modes.

and both bands were shifted to the lower-energy region. When the linear relationship between the frequency (ν) and charge on MeEDO-TTF (ρ) is assumed, ν is linked to ρ as follows:

$$\nu_9(\rho) = 1548 + 100(1-\rho)\ \text{cm}^{-1} \quad (1)$$

$$\nu_{10}(\rho) = 1503 + 118(1-\rho)\ \text{cm}^{-1} \quad (2)$$

Figure 7 also shows the infrared spectrum of **3** at room temperature (*L*-phase), C═C stretching region of which exhibited three absorption bands at 1625, 1558, and 1523 cm^{-1}. Although the observed spectrum is not the simple superposition of those of neutral and monocationic MeEDO-TTF molecules, it can be reasonably interpreted as the coexistence of charge-rich and -poor donor molecules. By analogy to the spectrum of (MeEDO-TTF)FeBr$_4$, the latter two bands are assigned to the ν_9 and ν_{10} modes of charge-

(23) Barszcz, B.; L£apiński, A.; Graja, A.; Flakina, A. M.; Chekhlov, A. N.; Lyubovskaya, R. N. *Chem. Phys.* **2006**, *330*, 486–494.
(24) Barszcz, B.; L£apiński, A.; Graja, A.; Flakina, A. M.; Zhilyaeva, E.; Yamada, J.; Lyubovskaya, R. *Synth. Met.* **2006**, *156*, 1043–1051.
(25) Nakano, Y.; Balodis, K.; Yamochi, H.; Saito, G.; Uruichi, M.; Yakushi, K. *Solid State Sci.* **2008**, doi: 10.1016/j.solidstatesciences.2008.01.020.

Table 5. Observed Frequencies (cm^{-1}) of Infrared Spectra in MeEDO-TTF, $(MeEDO\text{-}TTF)_2PF_6$, and (MeEDO-TTF)$FeBr_4$ at Room Temperature

	MeEDO-TTF	3[a]	(MeEDO-TTF)$FeBr_4$
ν_9	1648	1625? (P, $\rho = 0.2_3$)	
		1558 (R, $\rho = 0.9_0$)	1548
ν_{10}	1621	1625? (P, $\rho = -0.0_3$)	
		1523 (R, $\rho = 0.8_3$)	1503
ν_{11}	1531		
ν_{12}	1453		1460?
ν_{13}	1442		
ν_{14}	1436	1445	1442?
ν_{15}	1429		1429?
ν_{16}	1383	1380	1373
ν_{17}	1368		1345
ν_{18}	1360		
ν_{19}	1267	1273	1264?
ν_{20}	1241	1246	1239?
ν_{21}	1224		
ν_{22}	1224 (R)	1223	
	1197	1201 (P)	
ν_{23}		1183 (R)	1190
	1167 or 1161	1163 (P)	
ν_{24}	1111	1111	1114

[a] "P" and "R" indicate the charge-poor and -rich sites, respectively. ρ: estimated charge on a molecule.

rich species, respectively. Applying eqs 1 and 2, the charge on charge-rich MeEDO-TTF in **3**, ρ^R, is estimated to be $+0.9_0$ to $+0.8_3$. The band at 1625 cm^{-1} can be assigned either the ν_9 or ν_{10} modes of charge-poor MeEDO-TTF but cannot be alternatively assigned since the relative intensities of these absorption bands are modulated depending on the ionization degree. According to eqs 1 and 2, the assignments of this band to the ν_9 and ν_{10} modes result in the estimated charge for a charge-poor donor molecule, ρ^P, to be 0.2_3 and -0.0_3, respectively. Although it could not be detected by crystal structure analysis, infrared spectra demonstrate the charge disproportionation (CD) in **3** at room temperature (*L*-phase), which should be the origin of the semiconducting behavior.

Raman Spectra. The temperature-dependent Raman spectra of **3** were examined. The calculated and observed Raman spectra of MeEDO-TTF and (MeEDO-TTF)$FeBr_4$ in the C═C stretching region are compared in Figure 8. In this case, not only the ν_9 and ν_{10} but also the ν_{11} ones could be distinguished from other bands to provide the following relations under the assumption of a linear correlation between the vibrational frequency and the charge on a molecule.

$$\nu_9(\rho) = 1553 + 96(1-\rho)\ cm^{-1} \quad (3)$$

$$\nu_{10}(\rho) = 1531 + 93(1-\rho)\ cm^{-1} \quad (4)$$

$$\nu_{11}(\rho) = 1415 + 118(1-\rho)\ cm^{-1} \quad (5)$$

Figure 9 shows the temperature-dependent Raman spectra of **3** along with the spectra of the stable metallic $(MeEDO\text{-}TTF)_2ClO_4$ salt at room temperature. At 300 K, just below the transition temperature, the Raman spectrum of **3** showed a very broad band at 1200−1430 cm^{-1} with a dip at 1378 cm^{-1}, two sharp bands at 1531 and 1561 cm^{-1}, and a weak band at 1625 cm^{-1}. The dip at 1378 cm^{-1} is ascribable to the CH_3 bending ν_{16} mode, which is observed at the same frequency in the infrared spectrum (Figure 7 and also Figure S10 in Supporting Information).

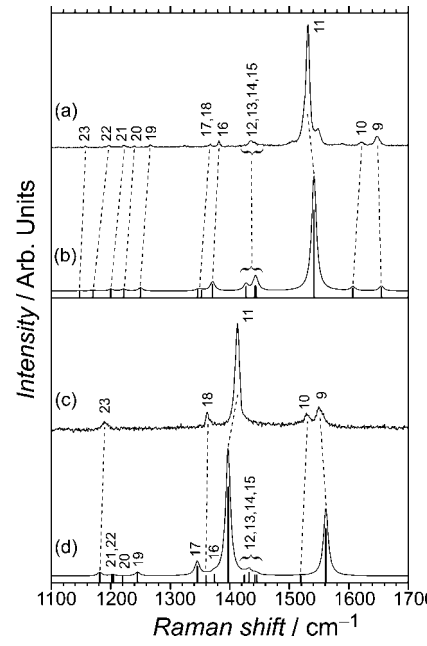

Figure 8. (a) Observed and (b) calculated Raman spectra of MeEDO-TTF. (c) Observed and (d) calculated Raman spectra of (MeEDO-TTF)$FeBr_4$. The excitation wavelength is 633 nm. Calculations were carried out at the B3LYP/6-31G(d,p) level of theory. Numbering of the bands corresponds to that of fundamental modes.

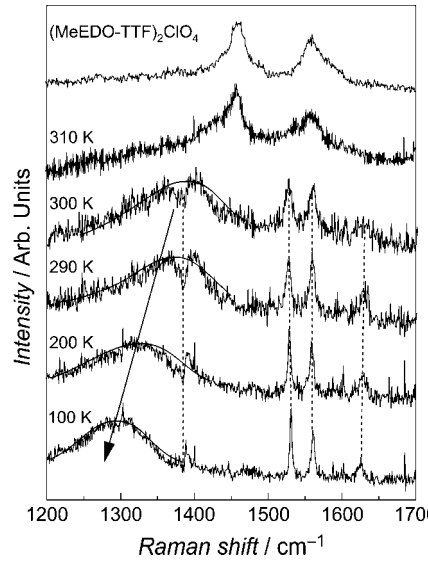

Figure 9. Temperature-dependent Raman spectra of the single crystal of **3** in the C═C stretching region, which are in the *H*-phase at 310 K and in the *L*-phase at other temperatures. For reference, the Raman spectrum of the metallic $(MeEDO\text{-}TTF)_2ClO_4$ is also shown at the top. The solid curves follow the broad bands are guides for the eye. The dashed lines point the dip ascribable to ν_{16} mode at 1378 cm^{-1} and the peaks at 1531, 1561, and 1625 cm^{-1}. The arrow shows the temperature variation of the ν_{11} band.

On cooling, a very broad band with the lowest energy showed a distinct shift to a lower frequency, whereas other bands exhibited primarily temperature-independent frequencies and became sharper at lower temperature. Comparing the vibrational spectra of MeEDO-TTF and (MeEDO-TTF)$FeBr_4$, the broad band that shifted to around 1300 cm^{-1} at 100 K is assigned to the ν_{11} mode of MeEDO-TTF. Although the frequency is much lower than that of monocationic donor molecule in (MeEDO-TTF)$FeBr_4$, a similar broad feature and large shift of the vibrational peaks were

Table 6. Estimated Site Charges (ρ) of (MeEDO-TTF)$_2$PF$_6$ at 100 K based on the Raman Spectra[a]

	1531 cm^{-1}	1561 cm^{-1}	1625 cm^{-1}
ν_9	(1.2_3)	$+0.9_2$	$+0.2_5$
ν_{10}	$+1.0_0$	$(+0.6_8)$	-0.0_1
ν_{11}	$+0.2_2$	(-0.2_4)	(-0.7_8)

[a] Unaccepted assignments are in brackets.

often observed for the ν_3 mode in ET salts.[26] The main contribution to the ν_3 mode of ET is the central C=C stretching mode, and the electron-molecular vibration ($e-mv$) interaction on the ν_3 mode is the maximum among the C=C stretching modes. The ν_{11} mode of MeEDO-TTF also consists primarily of the central C=C stretching. The observed spectral feature in **3** must stem from the large $e-mv$ interaction on the ν_{11} mode of MeEDO-TTF.

Table 6 summarizes the estimated charges on a donor molecule corresponding to the assignment of each vibrational mode based on the eqs 3−5. From the infrared spectrum of **3**, the molecular site charges are considered to be in the range from 0 to +1. Unacceptable assignments, based on which the site charge significantly deviates from this range, are shown in parentheses in Table 6. Although the assignment of 1561 cm^{-1} band to ν_{10} results in an estimated site-charge between 0 and +1, the value of $+0.6_8$ is inconsistent with the degree of the CD evaluated from the infrared spectra. The other calculated site charges show good correspondence to those derived from the infrared spectra, while an unequivocal assignment could not be performed due to the lack of a detailed vibrational study.

The spectrum at 310 K (*H*-phase) showed two broad bands at 1558 and 1456 cm^{-1}, similarly to that of the ClO_4 salt. Regarding the eqs 3−5, the former band can be assigned to ν_9 or ν_{10} mode and the latter one to ν_{11}. These assignments, however, resulted in estimated site-charges of of 0.9_5, 0.7_1, and 0.6_5, respectively, all of which are significantly larger than 0.5. Along with the broadness of the bands, it is unreasonable to assume that all donor molecules are uniformly charged in +0.5 in the *H*-phase of **3**. The broad feature of each band indicates that the charge is inhomogeneous at the molecular site but not completely localized (i.e., a nearly localized charge-disproportionated state).[26e]

The origin of the semiconductor−semiconductor transition from *H*- to *L*-phase in **3** is assigned to the development of the localization of the CD associated with structural modulation. This scenario corresponds well with the observed transport property of **3**. At metal−insulator transition temperatures due to charge ordering (CO), θ-type ET salts show more than 3 orders of resistivity jumps.[27] The smaller resistivity modulation observed in **3** than those in the ET salts is qualitatively understood as a result of nonmetal to nonmetal transition. However, the interpretation of the Raman spectra described above means that the nearly localized state is realized also in (MeEDO-TTF)$_2$ClO$_4$, while this salt shows metallic behavior down to 10 K (Although it is not shown in the figure, also another metallic salt (MeEDO-TTF)$_2$BF$_4$ showed very similar Raman spectra to that of the ClO_4 salt). The factor which discriminated the transport properties of **3** and ClO_4 salt is discussed in the following section.

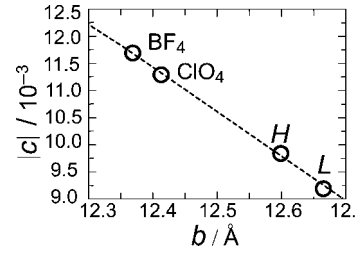

Figure 10. Relationship between the lattice constant *b* and the absolute value of the transverse intermolecular overlap integral *c* in (MeEDO-TTF)$_2$X (X = BF_4, ClO_4, and PF_6). *H* and *L* indicate the *H*- and *L*-phases of **3** at 302 K, respectively. The dashed line is a guide for eyes.

Comparison of Intermolecular Interactions. It is noteworthy that the areas of the conducting plane per formula unit agreed within a difference of less than 2% among the isostructural BF_4, ClO_4, and PF_6 (*H*-phase) complexes, while the former two and the last one showed different transport properties. These facts suggest that the electronic structures of these complexes are sensitive to the small modulation of the crystal structure. To highlight the relationship between the structural variation and the electronic structure of isostructural (MeEDO-TTF)$_2$X (X = BF_4, ClO_4, and PF_6 of the *H*-phase) salts, the sizes of the counter components were compared. The anion volume (V_A) was defined as the volume of the sphere, the radius of which was defined as the sum of the vdW of the outer atom and the averaged bond length between the central and outer atoms (see Figure S11 in Supporting Information). As shown in Table 4, V_A was increased in the sequence of BF_4, ClO_4, and PF_6.

Since the off-site Coulomb interaction (V) with respect to the magnitude of transfer integral (t) plays an important role in providing CD in a 1/4-filled system,[28] their relative variations are compared in this isostructural series. The increment of V_A caused the enhancements of the *b*- and *c*-axis lengths. Despite the small variation of the lattice constants, the magnitude of the overlap integral along the 0° direction (c) showed quick decrement, while those along the 60 and 120° directions (p and s) retained approximately the same values (Table 4, see also Figure S12 in Supporting Information). It is noteworthy that the variation in $|c|$ amounts to 20% for the small modulation of the *b*-axis length (ca. 2 %) as shown in Figure 10. This sensitive feature is regarded as the result of the moderately weak intermolecular interaction and the nature of t which decays exponentially as the function of intermolecular distance r. On the other hand, V is proportional to $1/r$. Although the relative orientation of the

(26) (a) Yamamoto, K.; Yakushi, K.; Miyagawa, K.; Kanoda, K.; Kawamoto, A. *Phys. Rev. B* **2002**, *65*, 085110/1−8. (b) Suzuki, K.; Yamamoto, K.; Yakushi, K. *Phys. Rev. B* **2004**, *69*, 085114/1−11. (c) Yamamoto, T.; Yakushi, K.; Shimizu, Y.; Saito, G. *J. Phys. Soc. Jpn.* **2004**, *73*, 2326–2332. (d) Yamamoto, T.; Uruichi, M.; Yakushi, K.; Yamaura, J.; Tajima, H. *Phys. Rev. B* **2004**, *70*, 125102/1−11. (e) Yamamoto, T.; Uruichi, M.; Yakushi, K. *Phys. Rev. B* **2006**, *73*, 125116/1−12. (f) Yamamoto, T.; Eda, J.; Nakao, A.; Kato, R.; Yakushi, K. *Phys. Rev. B* **2007**, *75*, 205132/1−18.

(27) (a) Mori, H.; Tanaka, S.; Mori, T. *Phys. Rev. B* **1998**, *57*, 12023–12029. (b) Mori, T.; Mori, H.; Tanaka, S. *Bull. Chem. Soc. Jpn.* **1999**, *72*, 179–197. (c) Yoshino, H.; Murata, K.; Saito, K.; Nishikawa, H.; Kikuchi, K.; Ikemoto, I. *Phys. Rev. B* **2003**, *67*, 035111/1-9.

(28) Seo, H.; Fukuyama, H. *J. Phys. Soc. Jpn.* **1997**, *66*, 1249–1252.

neighboring molecules under consideration was different from that in our case, it is reported that *V* can be evaluated rather correctly even assuming that the charge on each molecule is concentrated on its center when the intermolecular distance is around or bigger than the sum of vdW.[29] This type of approximation resulted in less than 3% decrement of *V* along the *b*-axis when the anion in (MeEDO-TTF)$_2$BF$_4$ was substituted by PF_6. These results indicate that the magnitude of *V*/*t* is increased in the order of BF_4, ClO_4, and PF_6 (*H*-phase) salt mainly due the modulation of the overlap integral *c*. It is suggested that the border between metal and semiconductor was determined by the magnitude of *V*/*t* and was located between ClO_4 and PF_6 (*H*-phase) salts.

The concept of chemical pressure[30] has been successfully applied to understand the relationship between the electronic structures and the lattice constants of the molecular conductors that exhibit approximately the same packing patterns of conducting components but have different counterparts.[27] The chemical pressure in (MeEDO-TTF)$_2$X (X = BF_4, ClO_4, and PF_6 (*H*-phase)) suggests that the compression of the lattice by employing small-sized anion stabilizes the metallic state. In fact, **3** showed stable metallic behavior down to 2 K by applying a hydrostatic pressure of 10 kbar.[31] Furthermore, the application of the uniaxial strain on this salt is of interest since the bulkiness of PF_6 caused the anisotropic negative pressure that affected more effectively along the *b*-axis than along the *c*-axis in the conducting layer.

Limitations of Measurements. As for the boundary between the metal and semiconductor in our isostructural salts, it is noteworthy that the transport properties were located at the border between ClO_4 and PF_6 (*H*-phase) salts, while these two species show very similar Raman spectra of a nearly localized CD state. These results demonstrate that vibrational spectroscopy is effective to detect the inhomogeneous distribution of the charge carriers on a chemical species. This method, however, would require more detailed processes to understand the relationship with the transport properties. As a similar example, β''-(ET)$_3$(ClO$_4$)$_2$ should be mentioned.[26e,32] At room temperature, this salt exhibits a metallic transport property, and the ν_{27} C=C vibrational mode observed in the conductivity spectra shows a broad band characteristic of a nearly localized CD state. The frequency, intensity, and width of this band are continuously modulated on cooling across T_{MI} (170.4 K) to turn into bands assignable to charge-rich and -poor components. Since the intensity of the ν_{27} mode of charge-poor site is small even at the lowest temperature reported (10 K), this salt shows very similar vibrational spectra in this frequency region between room temperature and just below T_{MI}, while the transport properties are obviously altered.

In addition to the comparison of the isostructural MeEDO-TTF salts, the comparison of the *H*- and *L*-phase of **3** is interesting. As is described above, the *L*-phase is characterized by the twisting of neighboring donor molecules, while all MeEDO-TTF are parallel to each other in the *H*-phase. The effects of the molecular displacements on the intermolecular interactions are discussed for θ-(ET)$_2$RbZn(SCN)$_4$.[33] In this case, the rotation of ET from the position in the metallic phase is claimed to be indispensable to provide the observed charge ordering (CO) pattern. By analogy to this salt, the twisting of the neighboring donor molecules in the *L*-phase of **3** is expected to play an important role in providing definite CD state from the nearly localized one of the *H*-phase, while the pattern of charge distribution is not clear yet.

One of the reasons why the CO pattern in **3** could not be determined by structural analysis may come from the number of donor molecules in a unit cell. In the metallic phase of θ-(ET)$_2$RbZn(SCN)$_4$, two donor molecules were accommodated in a donor layer in a unit cell, and the CO transition doubled the unit cell to form the stripes of charge-poor and -rich donor molecules approximately along the molecular short axis.[33] The multiplied unit cell provided satellite diffractions, the intensities of which were 0.01−0.1 times those of Bragg reflections. In the case of **3**, the cell doubling is not needed to form the stripes of charge-poor (and -rich) donor molecules either along the molecular short axis (along the interaction *c*) or along the stacking axis (along the interaction *s* or *p*), since four donor molecules are included in a donor layer per unit cell both in *H*- and *L*-phases. In this case, the intensity distribution of Bragg reflections must be affected, and the lower symmetry of the space group should be applied for the structural analysis which includes the CO pattern determination. The modulation, however, might be too faint to be detected by our diffractometer. Another possible reason to prevent the CO pattern determination is the coexistence of different types of CO patterns. Since one donor layer contains four MeEDO-TTF molecules in a unit cell, six patterns of arrangements of charge-poor and -rich molecules are possible without expanding the unit cell. When the different types of CO patterns are randomly included in a crystal, the crystal structure analysis shows the averaged structure. As was mentioned in the introductory part of this report, an example, in which the averaged structure is in conflict with the physical properties, had been reported for a salt of related compound, TP-EDOT.[12] Along with the results discussed for the isostructural series of the salts, the comparison of the *H*- and the *L*-phase of **3** demonstrates the sensitivity of the electronic structure of the MeEDO-TTF salt to the subtle crystal structure modulation.

Conclusion

The combination of MeEDO-TTF and PF_6 anion provided three kinds of 2:1 salts while polymorphism was rarely observed for the salts of other ethylenedioxy-TTF derivatives

(29) (a) Mori, T. *Bull. Chem. Soc. Jpn.* **2000**, *73*, 2243–2253. (b) Seo, H.; Hotta, C.; Fukuyama, H. *Chem. Rev.* **2004**, *104*, 5005–5036.

(30) (a) Hünig, S.; Sinzger, K.; Jopp, M.; Bauer, D.; Bietsch, W.; von Schütz, J. U.; Wolf, H. C. *Angew. Chem., Int. Ed. Engl.* **1992**, *31*, 859–862. (b) Aonuma, S.; Sawa, H.; Kato, R. *J. Chem. Soc., Perkin Trans.* **1995**, *2*, 1541–1549. (c) Aonuma, S.; Sawa, H.; Kato, R. *Synth. Met.* **1995**, *70*, 1089–1090.

(31) Detailed results will be published elsewhere.

(32) Enoki, T.; Tsujikawa, K.; Suzuki, K.; Uchida, A.; Ohashi, Y. *Phys. Rev. B* **1994**, *50*, 16287–16294.

(33) (a) Miyashita, S.; Yonemitsu, K. *Phys. Rev. B* **2007**, *75*, 245112/1−6. (b) Watanabe, M.; Noda, Y.; Nogami, Y.; Mori, H. *J. Phys. Soc. Jpn.* **2004**, *73*, 116–122.

in general. Among the MeEDO-TTF salts with PF_6, the black plate modification showed a semiconductor-to-semiconductor first-order phase transition just above room temperature (around 303 K). This means that this salt has the potential for the use in the molecular switching and/or memory system. Nearly localized and distinct charge disproportionations were observed by vibrational spectra in the high-temperature and low-temperature phases, respectively, while such disproportionations could not be detected by structural analyses in either phase. The comparison of the structural features of the isostructural MeEDO-TTF salts, the two-dimensional stable metals (MeEDO-TTF)$_2$X (X = BF_4, ClO_4), and the high-temperature phase of the PF_6 salt, demonstrated the sensitivity of the electronic structures of these MeEDO-TTF salts to the slight lattice modulations. In this series, the ratio of the magnitudes of neighboring site Coulomb repulsion (V) and the intermolecular transfer integral (t) was well correlated with the volume of anion while the effect was anisotropic. The anion size between those of ClO_4 and PF_6 is concluded to provide the border between metals and charge disproportionated semiconductors. The rotation of MeEDO-TTF associated with the phase transition of the PF_6 salt is noted since the molecular rotation is claimed to be indispensable to form a charge ordering pattern in an ET salt.

This study demonstrated the versatility and limitations of vibrational spectroscopy to examine charge-disproportionated systems: spectroscopy is sensitive to the inhomogeneity of the charge carriers as had been reported but cannot easily predict the transport property of a nearly localized state. Also, the difficulty to detect faint structural modulations by X-ray structural analysis was demonstrated. Despite these technical difficulties, the investigation of MeEDO-TTF salts provided a new phase transition system based on charge disproportionation. The molecular conductors with moderately weak intermolecular interactions is interesting to provide variety of complexes, the physical properties are driven by correlated electrons.

Experimental Section

General Details. IR and UV−vis spectra were measured on KBr pellets on Perkin-Elmer Paragon 1000 and Shimadzu UV-3100 spectrometers, respectively. Raman spectra were measured on 180° back-reflecting geometry with Renishaw Ramanscope System-1000. The excitation wavelength was 633 nm. The measurements were performed on single crystals for MeEDO-TTF, (MeEDO-TTF)$_2$$ClO_4$, and (MeEDO-TTF)$_2$$PF_6$ black plate modification, while that for (MeEDO-TTF)$FeBr_4$ was carried out on the KBr pellet. The conductivities were measured by the conventional four- and two-probe methods in the high- and low-temperature regions, respectively. Gold wires were attached to the samples using carbon paste (DOTITE XC-12, JEOL; solvent: diethyl succinate, TCI). The cooling rate was 0.5 K min^{-1}. Liquid nitrogen was employed as the reference for the thermocouple of the temperature controller. For **1** and **2**, the measurements were performed on compressed pellets, which were prepared by applying pressure of around 18 kg cm^{-2} and cut into rectangular shapes with the size of 1.4 × 0.5 × 0.2 mm^3. Gold wires with a diameter of 25 μm were employed. The lowest temperature we measured was 10 K. In the case of **3**, the temperature-dependent resistivities of the single crystals, to which gold wires with a diameter of 10 μm were attached, were measured down to 110 K. To confirm the first-order transition behavior of salt **3**, the temperature-dependent resistivity measurement for four single crystals was carried out by the conventional four-probe method in the temperature region of 295−315 K. The sample was cooled/heated in the rate of 0.2 K min^{-1} to the target temperatures, which were settled every 1 K, and kept for 5 min at the same temperature to maintain the thermal equilibrium in the cryostat. The resistances of the samples were recorded every 1 min. The width of the thermal hysteresis of the transition ranged from 1 to 1.5 K. The temperature dependence of the magnetic susceptibility of **1**, **2**, and **3** was measured on a SQUID magnetometer of Quantum Design MPMS-XL applying a magnetic field of 10 kOe. The data were corrected for the Curie impurities and core diamagnetism. The Curie constants for **1**, **2**, and **3** were 0.875, 1.1, and 0.072 × 10^{-3} emu K spin^{-1}, respectively. The core diamagnetism was estimated from the sum of the Pascal constants, which amounted to −3.27 × 10^{-4} emu spin^{-1} for (MeEDO-TTF)$_2$$PF_6$.[34]

The intermolecular overlap integrals (s) between the donor molecules were calculated by means of extended Hückel method on the basis of the crystal structures. The tight binding approximation afforded the dispersion relation and the Fermi surface under the assumption of $t = Es$, where t represents the transfer integral and $E = -10$ eV. The ζ-parameters of atomic orbitals were taken from ref 35 for oxygen and from ref 36 for other atoms. The 3d-orbitals of the sulfur atom were included in the calculation.

Synthesis. Modification **1** was prepared following the method in ref 13. The solvents for electro-oxidation were distilled from Mg/IB_{2B} and stored under nitrogen atmosphere. (BMI)PF_6 was prepared according to ref 37. The salts of **2** and **3** were prepared as follows. In a Pyrex glass H-shaped cell separated with a glass frit, MeEDO-TTF and (BMI)PF_6 were placed in the anodic and both compartments, respectively, under helium gas in a glovebox (H_2O, O_2 < 1 ppm). Two Pt wire electrodes (cathode: 2 mmϕ, anode: 1 mmϕ) passing through Teflon holder were placed on the necks of the glass cell and tightly sealed with paraffin films, and the cell was then placed under an ambient atmosphere. A constant current of 0.5 μA was passed through two electrodes for around 1 week at room temperature. In a typical procedure, MeEDO-TTF (ca. 10 mg) and (BMI)PF_6 (ca. 150 mg) were dissolved in 18 mL of *n*-propanol, and **2** was obtained as thin dark-green plates; using same amount of donor and solvent, while reducing the supporting electrolyte to ca. 70 mg, **3** was obtained as black plates with a typical size of 0.6 × 0.15 × 0.05 mm^3.

(MeEDO-TTF)$FeBr_4$ was prepared by mixing MeEDO-TTF (15 mg) and (Bu_4N)$FeBr_4$ (60 mg) in EtOH (18 mL), which afforded 13 mg of dark-green powder after being dried in vacuo overnight. On the basis of the composition of the elemental analysis and SEM-EDX, the composition of the dark-green powder was estimated to be MeEDO-TTF:$FeBr_4$ = 1:1. Elemental analysis: Found: C, 16.86; H, 1.38. Calcd for $C_9H_8O_2S_4FeBr_4$: C, 16.58; H: 1.24%. SEM-EDX: S:Fe:Br = 2.84(5):0.75(13):2.91(10) ≈ 4:1:4

X-ray Structure Determination. The data of **3** were collected on an imaging plate type diffractometer (MacScience DIP-2020K)

(34) Gupta, R. R. In *Landolt-Bornstein, New Series II*; Hellwege, K.-H., Hellwege, A. M., Eds.; Springer Verlag: Berlin, 1986; Vol. 16 (Diamagnetism Susceptibility).
(35) Summerville, R. H.; Hoffmann, R. *J. Am. Chem. Soc.* **1976**, *98*, 7240–7254.
(36) Mori, T.; Kobayashi, A.; Sasaki, Y.; Kobayashi, H.; Saito, G.; Inokuchi, H. *Bull. Chem. Soc. Jpn.* **1984**, *57*, 627–633.
(37) Huddleston, J. G.; Visser, A. E.; Reichert, W. M.; Willauer, H. D.; Broker, G. A.; Rogers, R. D. *Green Chem.* **2001**, *3*, 156–164.
(38) (a) Burla, M. C.; Caliandro, R.; Camalli, M.; Carrozzini, B.; Cascarano, G. L.; De Caro, L.; Giacovazzo, C.; Polidori, G.; Spagna, R. *J. Appl. Crystallogr.* **2005**, *38*, 381–388. (b) Sheldrick, G. M.; *SHELXS-97, A Program for Crystal Structure Refinement*; University of Göttingen, Göttingen, Germany, 1997; Release 97-2.

with graphite monochromated Mo Kα radiation. The temperature was controlled by a XR-CS10K cryostat (Japan Thermal Engineering) at a cooling/heating rate of 0.5 K min^{-1}. The accuracies of temperature settlements of our cooling system are ±0.8 and ±0.67 K for the temperature ranges below and above 273 K, respectively. At each specified temperature, the system retains the temperature within at most ±0.5 K. First, the crystal was cooled down to 110 K, and it was then warmed up to 302 K. The diffraction data were collected at 110, 150, 200, 250, 290, and 302 K in the heating process. After that, the crystal was warmed up from 302 to 342 K and then cooled down to 302 K. The diffraction data were collected at 342, 320, and 302 K in the cooling process. The structure was solved by a direct method of SIR2004[38a] and refined by a full matrix least-squares method on F^2 by means of Shelxl-97.[38b] Table 3 summarizes the parameters for crystals, data collections, and refinements. The positional parameters for all hydrogen atoms were obtained by differential synthesis and refined applying the isotropic temperature factors, except for the ethylene hydrogen atoms in the *H*-phase, which were ignored in the analysis.

Computational Details. All computations were performed with the Gaussian 03 program package[39] using the 6-31G(d,p) basis set.[40] Density functional theory (DFT) calculations were carried out using a hybrid method of Hartree−Fock and density functional theory (B3LYP), which combines Becke's three-parameter nonlocal exchange functional[41] with the correlation functional of Lee, Yang, and Parr.[42] In order to ensure the reliability of the frequencies, both "Opt=Tight" and "Int=Ultrafine" were specified. Calculated frequencies were scaled by the factor of 0.96 according to the literature.[43]

(39) Frisch, M. J.; et al. *Gaussian 03*, Revision C.02; Gaussian, Inc.: Wallingford, CT, 2004.
(40) Hehre, W. J.; Ditchfield, R.; Pople, J. A. *J. Chem. Phys.* **1972**, *56*, 2257–2261.
(41) (a) Becke, A. D. *Phys. Rev. A* **1988**, *38*, 3098–3100. (b) Becke, A. D. *J. Chem. Phys.* **1993**, *98*, 5648–5652.
(42) Lee, C.; Yang, W.; Parr, R. G. *Phys. Rev. B* **1998**, *37*, 785–789.
(43) Scott, A. P.; Radom, L. *J. Phys. Chem.* **1996**, *100*, 16502–16513.

Acknowledgment. This work was partly supported by Grants-in-Aid for Scientific Research on Priority Areas of Molecular Conductors (No. 15073215), 21st Century COE on Kyoto University Alliance for Chemistry (No. 15205019), from the Ministry of Education, Culture, Sports, Science and Technology, Japan, and for Creative Scientific Research (18GS0208) from JSPS.

Supporting Information Available: Full author list for ref 39. Figure S1, Typical photos of (MeEDO-TTF)$_2$PF$_6$ salts; Figure S2, Optical absorption spectra of the (MeEDO-TTF)$_2$PF$_6$ salts in the KBr pellets; Figure S3, Conformation of the PF_6 anion in the *L*-phase at different temperatures; Figure S4, Calculated and observed IR spectra of MeEDO-TTF; Figures S5 and S6, Calculated and observed Raman spectra of MeEDO-TTF; Figure S7, Calculated and observed IR spectra of monocationic salt (MeEDO-TTF)FeBr$_4$; Figures S8 and S9, Calculated and observed Raman spectra of monocationic (MeEDO-TTF)FeBr$_4$ salt; Figure S10, Comparison of the IR and Raman spectra of **3** in the low-temperature phase; Figure S11, Scheme for the calculation of the anion volume; Figure S12, Relationship between the absolute values of the intermolecular overlap integrals (*c*, *p*, and *s*) and the anion volumes (V_A) for (MeEDO-TTF)$_2$X (X = BF_4, ClO_4, and PF_6). Table S1, Calculated vibrational frequency and mode description of neutral and 1+ charged MeEDO-TTF; Table S2, Calculated and observed vibrational frequency of MeEDO-TTF and (MeEDO-TTF)FeBr$_4$ (PDF); CIF files for the crystal structure of the (MeEDO-TTF)$_2$PF$_6$ black plate modification. This material are available free of charge via the Internet at http://pubs.acs.org.

CCDC reference numbers: CCDC 680787, 680788, 680789, 680790, 680791, 680792, 680793, 680794, and 680795 for (MeEDO-TTF)$_2$PF$_6$ black plate modification under 110, 150, 200, 250, 290, 302 (heating), 302 (cooling), 320, and 342 K, respectively.

CM802517S